# Performance comparison of power fading mitigation techniques in multiband OFDM-UWB signals transmission along LR-PONs

**Tiago M. F. Alves*** **and Adolfo V. T. Cartaxo**

*Instituto de Telecomunicações, Department of Electrical and Computer Engineering, Instituto Superior Técnico, Technical University of Lisbon, 1049-001 Lisbon, Portugal*

**Corresponding author: tiago.alves@lx.it.pt*

Received February 15, 2013; accepted April 12, 2013; posted online July 26, 2013

The single sideband (SSB) modulation is assessed as a means to mitigate the dispersion-induced power fading on the distribution of ortogonal frequency division multiplexing (OFDM) ultra wideband (UWB) radio signals along long-reach passive optical networks (LR-PONs). Particularly, two different SSB architectures, namely, Sieben's architecture and four phase modulator (FPM) architecture are optimized to provide maximum sideband suppression. The minimum optical signal-to-noise ratio (OSNR) required to simultaneously distribute all the 14 OFDM-UWB sub-bands along the LR-PON distances ranging between 80 and 100 km is also evaluated through numerical simulation. FPM architecture is preferable over Sieben's architecture because the latter SSB architecture generates carriers-carriers beat term at the photodetector output with high power, thereby causing significant degradation in the OFDM-UWB sub-bands with lower central frequencies. The simultaneous distribution of the 14 SSB OFDM-UWB sub-bands in the LR-PON using the FPM architecture shows a minimum OSNR penalty of 3 dB compared with the centralized dispersion compensation technique.

*OCIS codes:* 060.0060, 060.2330.
*doi: 10.3788/COL201311.080602.*

The transmission performance impairments of ultra wideband (UWB) radio signals in optical fiber access infrastructures is a hot research topic[1−4]. Among the different transmission impairments, the fiber dispersion-induced power fading is identified as one of the most restrictive limitations on the performance of double sideband (DSB) ortogonal frequency-division multiplexing (OFDM) UWB signal transmission in intensity modulation-direct detection systems[5].

Several techniques were proposed to mitigate the dispersion-induced power fading. The most interesting techniques from complexity and performance viewpoints are based on single sideband (SSB) modulation[4], chirped electro-optic modulators (EOMs)[6], and centralized optical dispersion compensation (DC)[7].

The solution based on chirped EOMs showed reasonable tolerance to power fading degradation when the first three UWB sub-bands were transmitted simultaneously[6].

When SSB modulation of OFDM-UWB radio signals is employed, the power fading limitation is avoided because only a signal sideband is transmitted. The main disadvantage of SSB modulation is that, if a wavelength division multiplexing (WDM) technique is used to deliver the UWB services to different users with acceptable bandwidth requirements in both the optical line termination (OLT) and optical network units (ONUs)[8], one EOM structure per user is required and the cost of the SSB modulation cannot be shared among all the users served by the OLT.

If the DC is performed at the OLT or at the remote node (RN) of the LR-PON, its implementation cost may be shared by all the users served by the OLT, thus making it an attractive solution for the network operators. However, the implementation of DC LR-PONs is also challenging. For instance, giving that the dispersion compensator can fully compensate for the dispersion only for an ONU located at a given distance from the OLT, other ONUs still suffer from power fading degradation induced by the residual dispersion of the network[7].

Despite the different advantages and drawbacks of the aforementioned SSB modulation and DC techniques, the comparison of the transmission performance of multiband OFDM-UWB radio signals along LR-PONs employing these two techniques has yet to be performed. Hence, in this letter, the transmission of SSB OFDM-UWB radio signals as a solution to overcome the dispersion impairment of LR-PONs is assessed by numerical simulation, while considering the simultaneous transmission of the 14 UWB sub-bands. Additionally, the performance obtained when SSB OFDM-UWB radio signals are transmitted is compared with that achieved when optical DC is employed, from which the most promising solution from the technical viewpoint is identified.

Several EOMs architectures were proposed to generate SSB signals[9−11]. Some of these architectures are remarkably complex and expensive and, consequently, are not the most ideal options for use in access networks. Hence, in this letter, only the following (simpler) SSB architectures are investigated: i) the one proposed in Ref. [10], which uses one Mach-Zehnder modulator (MZM) followed by a phase-modulator (PM); ii) the one proposed in Ref. [11], consisting of a MZM with a MZM inserted in each arm. Henceforth, the former is designated by Sieben's architecture, while the latter is designated by four phase modulator (FPM) architecture.

 © 2013 Chinese Optics Letters

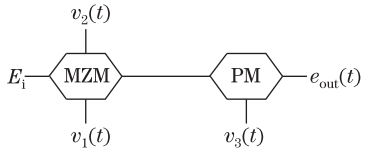


Fig. 1. Block diagram of Sieben's architecture.

Figure 1 shows the schematic diagram of Sieben's architecture used to generate SSB signals. This architecture consists of one dual arm MZM followed by a PM. The optical field at the output of the PM can be written as[10]

$$e_{\rm out}(t) = \frac{E_{\rm i}}{2}\Big[\exp\Big(\mathrm{j}\frac{\pi}{2V_x}v_1(t)\Big) + \exp\Big(\mathrm{j}\frac{\pi}{2V_x}v_2(t)\Big)\Big]\exp\Big(\mathrm{j}\frac{\pi}{2V_x}v_3(t)\Big), \quad (1)$$

where $V_x$ is the switching voltage (voltage level required to switch between the maximum and the minimum of the power transmission characteristic of the modulator); $v_1(t)$ and $v_2(t)$ are the voltage signals applied to the two arms of the MZM, respectively; $v_3(t)$ is the voltage signal applied to the PM.

The SSB version of a DSB signal, $x(t)$, is obtained from $x_{\rm SSB}(t) = x(t) \pm \mathrm{j}\, x_{\rm H}(t)$, where $x_{\rm H}(t)$ is the Hilbert transform (HT) of $x(t)$. Ideally, the HT transfer function, $H_{\rm H}(f)$, is given by $H_{\rm H}(f) = -\mathrm{j}\ \mathrm{sgn}(f)$, where $\mathrm{sgn}(f)$ is the signum function. Thus, in order to obtain sideband suppression, the voltage signals applied to the MZM arms are given by[10] $v_1(t) = -V_{\rm b} + v(t)$, $v_2(t) = +V_{\rm b} - v(t)$, $v_3(t) = v_{\rm H}(t)$, where $V_{\rm b}$ is the MZM bias point, $v(t)$ is the OFDM-UWB signal, and $v_{\rm H}(t)$ is the HT of $v(t)$.

Figure 2 shows the schematic diagram of the FPM architecture used to generate SSB signals. The FPM architecture consists of a MZM with a MZM inserted in each arm. The optical field at the output of the FPM architecture is given by[11]

$$e_{\rm out}(t) = \frac{E_{\rm i}}{2}\Big[\exp\Big(\mathrm{j}\frac{\pi}{2V_x}V_3\Big)\frac{e_1(t)}{E_{i,1}} + \exp\Big(-\mathrm{j}\frac{\pi}{2V_x}V_3\Big)\frac{e_2(t)}{E_{i,2}}\Big], \quad (2)$$

where $E_{\rm i,1}$ and $E_{\rm i,2}$ are the input optical fields of MZMs 1 and 2, respectively, and $V_3$ is a direct-current voltage used to control the phase shift between the signals obtained from the inner MZMs. In addition, $e_1(t)$ and $e_2(t)$ are the optical fields at the outputs of MZMs 1 and 2,

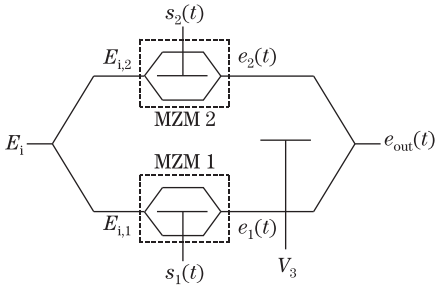


Fig. 2. Block diagram of the generation of SSB signals using FPM architecture.

respectively, which are given by

$$e_1(t) = \frac{E_{\rm i,1}}{2}\Big[\exp\Big(\mathrm{j}\frac{\pi}{2V_x}s_1(t)\Big) + \exp\Big(-\mathrm{j}\frac{\pi}{2V_x}s_1(t)\Big)\Big], \quad (3)$$

$$e_2(t) = \frac{E_{\rm i,2}}{2}\Big[\exp\Big(\mathrm{j}\frac{\pi}{2V_x}s_2(t)\Big) + \exp\Big(-\mathrm{j}\frac{\pi}{2V_x}s_2(t)\Big)\Big], \quad (4)$$

where $s_1(t)$ and $s_2(t)$ are the voltage signals applied to MZMs 1 and 2. These voltage signals can be written as $s_1(t) = -V_{\rm b,1} + g_1 v(t)$, $s_2(t) = -V_{\rm b,2} + g_2 v_{\rm H}(t)$, where $V_{\rm b,1}$ and $V_{\rm b,2}$ are the bias voltages of MZMs 1 and 2, respectively, and $g_1$ and $g_2$ are voltage gains used to adjust the level of the OFDM-UWB signal applied to the MZMs arms.

Figure 3 depicts the schematic diagram of the transmission of OFDM-UWB radio signals along the LR-PONs. The diagram represents the downstream transmission between the OLT located at the central office and the ONU located at the premises of the user.

The OFDM-UWB signals were generated accordingly with ECMA standard[12]. Quadrature phase shift keying (QPSK) was used for symbol mapping and, as a consequence, the maximum bit-rate of each OFDM-UWB signal was set at 640 Mb/s. Each of the OFDM-UWB sub-bands was generated separately and the time waveforms (32 OFDM-UWB symbols are considered for each band) obtained at the output of the different OFDM-UWB transmitters were added before being applied to the SSB EOM. The 14 OFDM-UWB sub-bands occupy the frequency range between 3.1 and 10.6 GHz[12]. We considered the two architectures described above to generate the SSB signals, and the HT was implemented

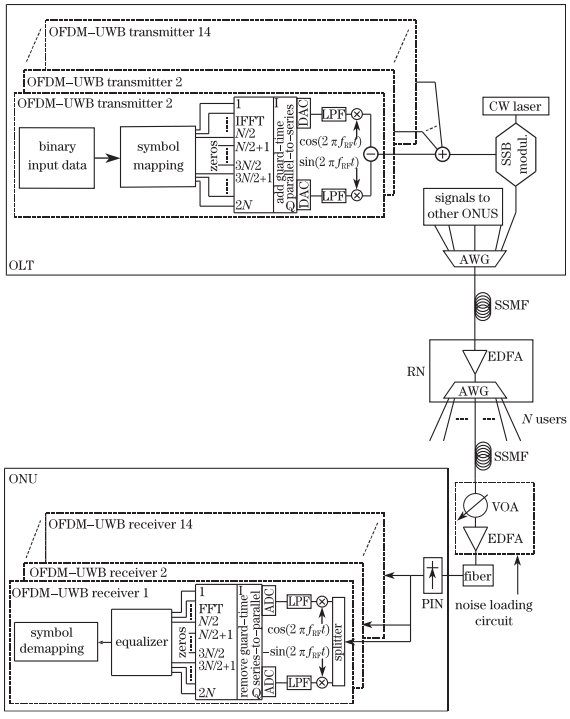


Fig. 3. Schematic diagram of the downstream distribution of OFDM-UWB radio signals along the LR-PON. ADC: analogue-to-digital converter; AWG: arrayed waveguide grating; DAC: digital-to-analogue converter; EDFA: Er-doped fiber amplifier; FFT: fast-Fourier transform; IFFT: inverse FFT; VOA: variable optical attenuator.

using a hybrid coupler with –1.5-dB bandwidth of 15.4 GHz (pass-band between 0.6 and 16 GHz) and phase variation along the pass-band not exceeding 8°. Experimental data of the hybrid coupler transfer function were used to model the hybrid coupler in the simulator. The operating optical wavelength, $\lambda$, was 1552.52 nm. After performing electro-optic conversion, the OFDM-UWB optical signal was launched into a feeder standard single-mode fiber (SSMF) with a length of 80 km. This fiber span represents the link between the OLT and the RN. After the RN, the optical signal was launched into another SSMF span with variable length (between 0 and 20 km). This span emulates the fiber distribution length required to connect the different users (ONUs) to the RN. The average optical power launched into the SSMF spans was 0 dBm in order to assume linear fiber propagation regime. At the optical receiver side, a noise loading circuit was used to adjust the OSNR level (defined in a reference bandwidth of 0.1 nm), a 2nd-order super-Gaussian optical filter with a –3-dB bandwidth of 30 GHz was used to reduce the amplified spontaneous emission (ASE) noise power, and the optical signal was photo detected. The responsivity was 1 A/W, and the absence of bandwidth limitation was considered for the PIN model. At the OFDM-UWB receiver side, the I and Q signal components were down-converted and filtered using 6th-order Bessel low-pass filters (LPFs) before being digitized. The OFDM-UWB signal was then demodulated and the pilots information of each OFDM-UWB sub-band was used to compensate for the distortions induced by the channel. The system performance was assessed by evaluating the bit error ratio (BER) using the semi-analytical Gaussian approach (SAGA)[13].

In the first step, the performance of the distribution of SSB OFDM-UWB radio signals in LR-PONs is assessed in back-to-back operation in order to gain insight into the most promising MZMs bias voltages. The performance optimization was performed using two figures of merit, namely, the BER evaluated from SAGA and the sideband suppression power ratio (SSPR). The SSPR was measured at the output of the SSB architecture, which allowed the quantification of the level of sideband suppression. In decibel, the SSPR is given by

$$\mathrm{SSPR} = \min_{i} \left[ 10 \lg \left( \frac{p_{\mathrm{ns}}^{(i)}}{p_{\mathrm{s}}^{(i)}} \right) \right], \tag{5}$$

where $p_{\mathrm{ns}}^{(i)}$ and $p_{\mathrm{s}}^{(i)}$ are the powers of the non-suppressed and suppressed sidebands, respectively, of the OFDM-UWB signal transmitted in the $i$th UWB band, and $1 \leqslant i \leqslant 14$ ($i \in \mathbb{N}$), depending on the UWB sub-band being transmitted.

The study as follows is performed considering the SSB generation using the Sieben's architecture.

Figure 4 depicts contour plots of the SSPR and BER as functions of the modulation indexes of the MZM and the PM. Three different MZM bias points were considered (the most interesting from the combination of SSPR and BER viewpoints), and the OSNR was set to 30 dB. The modulation indexes of the MZM and PM were defined, respectively, as $m_{\mathrm{MZ}}=V_{\mathrm{RMS,MZ}}/V_x$ and $m_{\mathrm{PM}}=V_{\mathrm{RMS,PM}}/V_x$. Here, $V_{\mathrm{RMS,MZ}}$ and $V_{\mathrm{RMS,PM}}$ are the RMS voltages of the signals $v(t)$ and $v_{\mathrm{H}}(t)$ applied to the MZM and PM arms, respectively.

Figures 4(a)–(d) show that the sideband suppression level is significantly dependent on the modulator bias point and on the signal levels applied to the EOMs. This is attributed to the very specific relation between the voltage levels of the signal and its HT required to achieve the SSB condition. The comparison between the SSPR and the BER results shown in Fig. 4 for the different bias point situations also shows that Sieben's architecture may be suitably designed to reach maximum sideband suppression, but it may not lead to the best system operation in terms of BER. This is because the maximum sideband suppression is achieved for bias voltages and modulation indexes levels that lead to different distortion levels. Therefore, the most promising parameters of Sieben's architecture result from the compromise between sideband suppression and BER.

From the results presented above, two different bias point cases are identified as the most promising, namely, i) $V_{\mathrm{b}}=0.5V_x$ (conventional QBP), which allows the reduction of the implementation complexity of such architecture by requiring similar voltage levels applied to the MZM and PM to achieve maximum sideband suppression, and ii) $V_{\mathrm{b}}=0.75V_x$, which allows obtaining lower BER levels in Fig. 4. Afterwards, these two cases are further analyzed considering fiber transmission.

It should be stressed that slightly lower BER levels (than for $V_{\mathrm{b}}=0.75V_x$) may be obtained for bias voltages closer to the minimum bias point ($V_{\mathrm{b}}=V_x$). However, in that case, the tolerance of the BER to bias voltage deviations is smaller and higher sensitivity to environmental conditions is expected in actual systems.

We consider the SSB generation using FPM architecture as follows. The optimization of the SSPR and BER was performed considering the MZMs 1 and 2 biased at different levels and for different modulation indexes. The

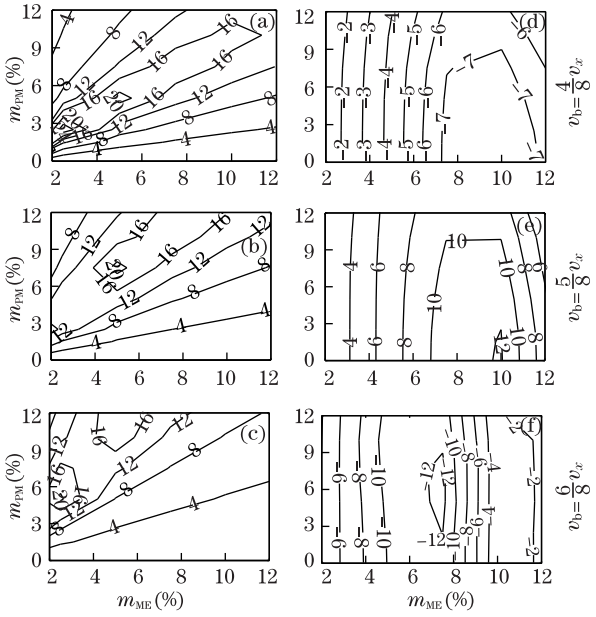


Fig. 4. Contour plots of (a), (b), and (c) SSPR and (d), (e), and (f) BER as functions of the modulation indexes of MZM and PM, considering different modulator bias points. In (d), (e) and (f), OSNR=30 dB. The SSB modulation is realized by Sieben's architecture.

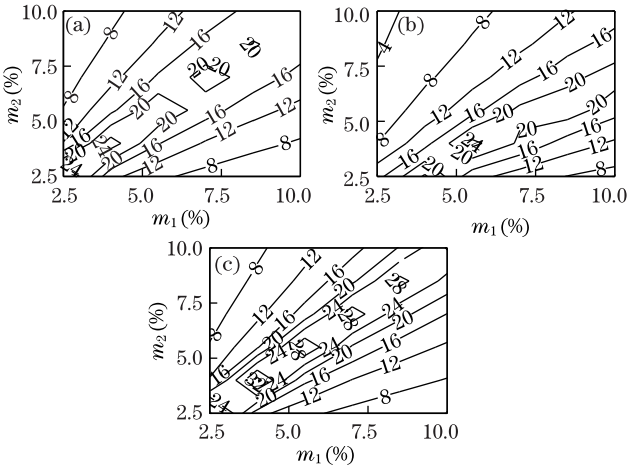


Fig. 5. Contour plots of the SSPR as functions of the modulation indexes of MZMs 1 and 2, for three different sets of bias voltages of (a) $V_{\mathrm{b},1} = \frac{4}{8}V_x$ and $V_{\mathrm{b},2} = \frac{4}{8}V_x$; (b) $V_{\mathrm{b},1} = \frac{4}{8}V_x$ and $V_{\mathrm{b},2} = V_x$; (c) $V_{\mathrm{b},1} = \frac{4}{5}V_x$ and $V_{\mathrm{b},2} = \frac{4}{5}V_x$. The SSB modulation is realized by FPM architecture.

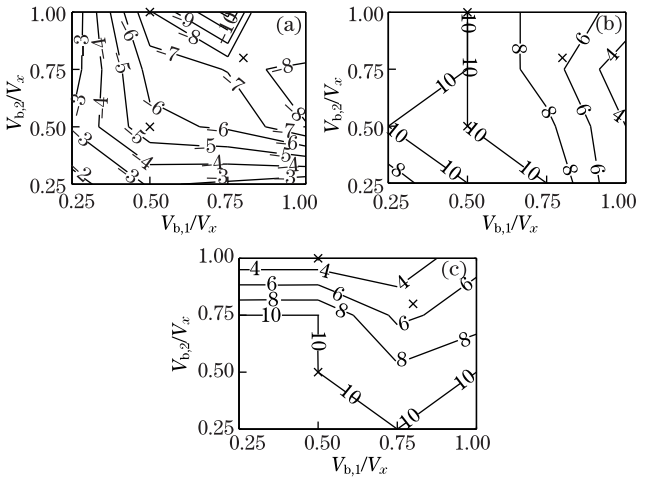


Fig. 6. Contour plots of (a) minimum BER, (b) optimum modulation index of MZM 1, and (c) optimum modulation index of MZM 2, as functions of the bias points of MZMs 1 and 2. OSNR=30 dB. The crosses represent the three cases presented in Fig. 5. The SSB modulation is realized by FPM architecture.

modulation indexes of MZMs 1 and 2 were defined as $m_1$=$V_{\mathrm{RMS},1}/V_x$ and $m_2$=$V_{\mathrm{RMS},2}/V_x$, respectively, where $V_{\mathrm{RMS},1}$ and $V_{\mathrm{RMS},2}$ are the RMS voltages of the signals $g_1 v(t)$ and $g_2 v_{\mathrm{H}}(t)$. The bias point of the MZM 3 was set to $V_x/2$ in order to produce a phase shift of $\pi/2$ between the signal and its HT.

Figure 5 depicts the SSPR as functions of the modulation indexes of MZMs 1 and 2. Although the study has been performed for several bias point levels of MZM 1 and 2, Fig. 5 only shows the results for three sets of bias points. The selection was performed by considering the SSPR and the BER levels, and the corresponding modulation indexes required. Figures 5(a) and (c) show that maximum sideband suppression is reached when the modulation indexes of MZMs 1 and 2 are identical. Instead, Fig. 5(b) shows that the optimized SSPR is obtained when the modulation index of MZM 2 is lower than that of MZM 1. This is due to the unbalance between the signal and its HT after electro-optic conversion, which is caused by the different modulators bias points. For the situation presented in Fig. 5(b), the relation between the modulation indexes of the two modulators, which leads to higher sideband suppression, is $m_2 = (\sqrt{2}/2)m_1$ because it allows obtaining the OFDM-UWB signal and its HT, respectively, at the outputs of MZMs 1 and 2, with the same average optical power.

Figure 6(a) shows the BER as a function of the bias points of MZM 1 and 2. For each bias point pair, the BER is the minimum one, i.e., it is chosen from partial results where the BER is evaluated for different modulation indexes of the two modulators, from which the best one is identified. Figure 6(a) shows that the three situations identified in Fig. 5 may not be the best ones in terms of BER. However, they represent a good compromise between the performance obtained from the SSPR and BER metrics. Figures 6(a) and (c) show the optimum modulation indexes of MZMs 1 and 2, respectively, corresponding to the BER levels shown in Fig. 6(a). The main outcome of these results follows from the comparison with the results of Fig. 5. In case of Figs. 5(a) and (c), the optimum modulation indexes corresponding to the BER optimization are very similar to the ones required to obtain high SSPR levels. In case of Fig. 5(b), the optimum modulation indexes corresponding to the BER optimization are slightly different from the ones required to obtain maximum sideband suppression.

The performance of SSB OFDM-UWB radio signal distribution along fiber lengths indicated for LR-PONs was assessed considering the two SSB architectures mentioned above. Particularly, the minimum required OSNR and the corresponding optimum modulation index required to achieve BER=$10^{-9}$ were evaluated for LR-PONs ranged between 80 and 100 km (i.e., the distance between the RN and ONUs ranging between 0 and 20 km). In the following, the BER (calculated using SAGA) is shown for the UWB sub-band with worst performance.

Sieben's architecture was analyzed considering i) $V_{\mathrm{b}}$=$0.5V_x$ and ii) $V_{\mathrm{b}}$=$0.75V_x$. In the former, the modulation index of the PM was set to make it equal to that of the MZM, while in the latter, the modulation index of the PM was set to be twice that of the MZM.

Figure 7 shows the power spectral density (PSD) of the OFDM-UWB signal at the PIN input and at the PIN output, considering back-to-back operation and a LR-PON comprising 90 km of SSMF. Sieben's architecture was employed considering $V_{\mathrm{b}}$=$0.5V_x$. Figures 7(a) and (c) confirm that a SSB signal with high sideband suppression is obtained with this configuration. However, contrary to the back-to-back case (Fig. 7(b)), Fig. 7(d) shows significant distortion components appearing at low frequencies. Moreover, part of these distortion components fall within the first UWB sub-bands and may preclude the transmission of information in these bands with acceptable performance. Further investigation showed that these distortion components are due to the 2nd-order nonlinearity terms generated by the EOMs and the PIN (notice that 2nd-order terms of the signal and of its HT are generated). In back-to-back operation, the power of these components is lower because i)

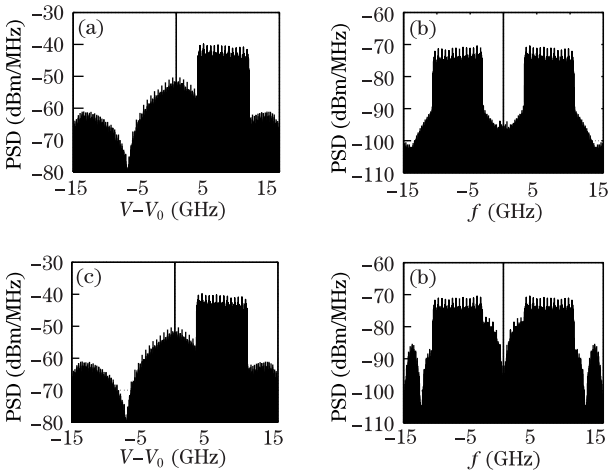


Fig. 7. PSD of the OFDM-UWB signal at (a), (c) PIN input and (b), (d) PIN output. (a) and (b) Back-to-back operation; (c) and (d) LR-PON with SSMF length of 90 km. The modulation index of the MZM is 5% and the SSB generation based on Sieben's architecture is employed.

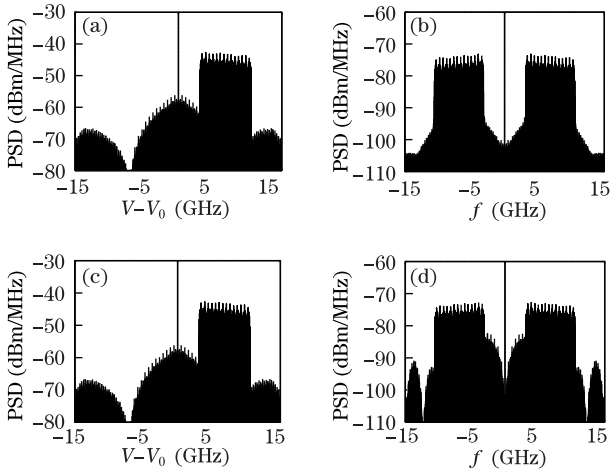


Fig. 8. PSD of the OFDM-UWB signal at (a), (c) PIN input and (b), (d) PIN output. (a) and (b) Back-to-back operation; (c) and (d) LR-PON with a SSMF reach of 90 km. The modulation indexes of the MZMs 1 and 2 are set to 5% and the SSB generation based on FPM architecture is employed.

the 2nd-order terms generated by the MZM modulator are canceled with the 2nd-order terms generated by the square law PIN detection, and ii) the distortion terms generated by the phase modulation in back-to-back operation are disregarded by the direct detection process.

Further investigation on the system performance optimization showed that an OSNR penalty due to fibre transmission higher than 6 dB is obtained when Sieben's architecture is employed to generate SSB signals. This penalty is significantly higher than that obtained by other solutions considered to mitigate the power fading, as shown latter in this work. This penalty is attributed to the distortion induced by the signal-signal beat terms. This limitation is not identified as a remarkable issue in previous proposed systems employing Sieben's architecture because they are mainly based on conventional digital signal transmission. In this case, the tolerance to distortion-induced degradation is quite different from the tolerance of OFDM-based systems, which cannot be understood as pure digital systems.

FPM architecture was assessed based on the following three cases: i) $V_{\mathrm{b},1}$=$V_{\mathrm{b},2}$=$0.5V_x$ (i.e., the QBP case),ii) $V_{\mathrm{b},1}$=$V_{\mathrm{b},2}$=$0.8V_x$ (i.e., the quasi-minimum bias point (QMBP)case), and iii) $V_{\mathrm{b},1}$=$0.5V_x$ and $V_{\mathrm{b},2}$=$V_x$ (i.e., the unbalanced bias point (UBP) case).

FPM architecture also suffers from distortion induced by the 2nd order terms due to the system nonlinearity. However, its impact on system performance is lower than in the case of Sieben's architecture due to the lower power levels involved. Figure 8 depicts the PSD at the PIN input and at the PIN output for the SSB generation performed using FPM architecture, considering the MZMs 1 and 2 biased at the quadrature point and the modulation indexes of MZMs 1 and 2 set to 5%. The comparison between Fig. 8 and Fig. 7 confirms the lower distortion power level obtained when FPM architecture is used. Indeed, when a LR-PON with 90 km of SSMF is considered, the margin between the PSD of the distortion component, which appears just close to the first UWB sub-band, and the maximum PSD of the first UWB subband is ∼4 dB lower in Sieben's than in FPM architecture.

As for Sieben's architecture, the optimization of the modulation index and the evaluation of the minimum OSNR required to achieve a BER=$10^{-9}$ were also performed for FPM architecture considering LR-PONs whose reaches range between 80 and 100 km.

Figure 9(a) shows the optimum modulation index of MZM 1 employed in the FPM architecture as a function of the LR-PON reach. The results are presented for the three bias point cases under analysis. In the QBP and the QMBP cases, $m_2$=$m_1$, whereas in the UBP case, $m_2$=$\sqrt{2}/2\times m_1$. As shown in Fig. 9(a), the following two main outcomes are drawn: i) the optimum modulation index does not depend on the LR-PON reach being considered, and ii) the optimum modulation index depends on the modulator bias point. The former is important from the viewpoint of the operator as it allows the distribution of the OFDM-UWB sub-bands to ONUs located at different distances from the OLT using the same voltage level for the signal applied to the EOM. The latter is attributed mainly to two different effects, namely, i) different bias points lead to different distortion levels induced by the system (EOM and PIN) nonlinearities, and ii) different bias points lead to different carrier-to-signal power ratio (CSPR) levels[14] and, consequently, leading to different optical average power levels of the OFDM-UWB signal at the FPM architecture output.

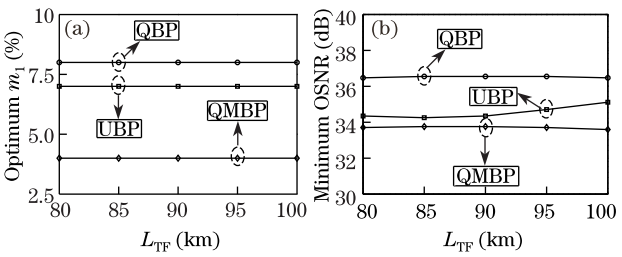


Fig. 9. (a) Optimum modulation index of MZM 1 and (b) minimum OSNR as a function of the total length of the LR-PON employing FPM architecture to generate SSB signals. The simultaneous transmission of the 14 UWB sub-bands is considered.

Figure 9(b) depicts the minimum OSNR required to achieve a BER of $10^{-9}$ corresponding to the modulation indexes presented in Fig. 9(a). Meanwhile, Fig. 9(b) shows that the different bias point cases under analysis require different OSNR levels to reach BER=$10^{-9}$. The lower OSNR is obtained for the QMBP, which is due to the tolerance to the degradation induced by the system nonlinearity and due to the lower CSPR[14].

Further investigation showed that, compared with the minimum OSNR required in back-to-back operation, OSNR penalties of 2.7, 2.3, and 1 dB are obtained for the QBP, UBP, and the QMBP cases, respectively. These penalties are attributed to the combined effect of residual power fading (due to the unperfect sideband suppression and fibre dispersion), and the combined EOM and PIN nonlinearity.

In a previous work, the impact of using optical DC at the RN to mitigate the degradation due to power fading is assessed through numerical simulation[7]. In that work, a dispersion-compensating fiber (DCF) was used at the RN, which was designed to compensate 90 km of SSMF. This means that, on the other hand, if the total distance between the OLT and a given ONU is 100 km, that ONU would still suffer from a power fading penalty induced by a positive residual dispersion corresponding to 10 km of SSMF. On the other hand, if the total OLT-ONU distance is 80 km, the ONU would suffer from a power fading penalty induced by a negative residual dispersion also corresponding to the absolute value of dispersion of 10 km of SSMF.

The analysis performed in Ref. [7] is accomplished under system conditions identical to the ones described in the current work for the SSB study. Therefore, a direct comparison between the results obtained by both power fading mitigation techniques may be performed. Notice that, a standard MZM biased at the quadrature point and the transmission of DSB OFDM-UWB signals are considered[7].

The results of Ref. [7] show that a minimum OSNR close to 31 dB is required to achieve BER=$10^{-9}$ in the OFDM-UWB sub-band showing worst performance. Additionally, a minimum OSNR degradation not exceeding 0.3 dB, compared with the full compensation scheme, is reached for a residual dispersion range close to 400 ps/nm (corresponding to a RN-ONU distance range between 0 and 20 km). Hence, compared with the minimum OSNR required by the SSB OFDM-UWB solution showing better performance (Fig. 9, QMBP case), the transmission of DSB OFDM-UWB signals along the LR-PONs employing DC leads to an OSNR improvement that achieves almost 3 dB. Moreover, compared with the QBP case, the OSNR improvement exceeds 5 dB.

In conclusion, the transmission of SSB OFDM-UWB radio signals is analyzed as a means to mitigate the dispersion impairment of the distribution of OFDM-UWB radio signals in LR-PONs. Due to their reduced complexity, two architectures to generate SSB OFDM-UWB radio signals are selected and discussed, namely, (i) Sieben's architecture, which employs one MZM and one PM, and (ii) the FPM architecture, which consists of a MZM with a MZM inserted in each arm. Sieben's architecture shows, when fiber transmission is considered, an OSNR penalty of 6 dB relative to back-to-back operation. This remarkable degradation is due to the very high power of the 2nd-order distortion components at the PIN output, which leads to significant degradation of the OFDM-UWB signals transmitted in the UWB bands with lower central frequencies. The transmission of SSB OFDM-UWB signals along LR-PONs employing FPM architecture shows an OSNR degradation close to 3 dB compared with the solution based on the DSB OFDM-UWB signal transmission and DC performed at the RN. This OSNR degradation combined with other advantages identified for dispersion-compensated LR-PONs (i.e., as system cost savings and higher tolerance to phase noise effects) suggest that the most promising solution to mitigate the fiber dispersion-induced power fading in LR-PONs is to use optical DC rather than to use SSB modulation.

The work was supported by Fundação para a Ciência e a Tecnologia from Portugal under contract SFRH/BD/29871/2006 and the project TURBO-PTDC/EEA-TEL/104358/2008. This work was also supported in part by the European FIVER-FP7-ICT-2009-4-249142 project.

## References

1. R. Llorente, T. Alves, M. Morant, M. Beltran, J. Perez, A. Cartaxo, and J. Marti, Photon. Technol. Lett. **20,** 945 (2008).
2. M. Thakur, T. Quinlan, S. Anas, D. Hunter, S. Walker, D. Smith, A. Borghesani, and D. Moodie, in *Proceedings of Optical Fibre Communication Conference 2009* OTuJ2 (2009).
3. P. Lombard, Y. Guennec, G. Maury, E. Novakov, and B. Cabon, J. Lightwave Technol. **27,** 1072 (2009).
4. M. Sakib, B. Hraimel, X. Zhang, K. Wu, T. Liu, T. Xu, and Q. Nie, J. Opt. Commun. Netw. **2,** 841 (2010).
5. T. Alves and A. Cartaxo, Photon. Technol. Lett. **21,** 158 (2009).
6. T. Alves, M. Morant, A. Cartaxo, and R. Llorente, IEEE J. Sel. Area Commun. **29,** 1311 (2011).
7. T. Alves and A. Cartaxo, J. Lightwave Technol. **29,** 2467 (2011).
8. C. Rodrigues, A. Gamelas, F. Carvalho, and A. Cartaxo, in *Proceedings of International Conference on Transparent Optical Networks 2011* 1 (2011).
9. K. Tanaka, K. Takano, K. Kondo, and K. Nakagawa, Electron. Lett. **38,** 133 (2002).
10. M. Sieben, J. Conradi, and D. Dodds, J. Lightwave Technol. **17,** 1742 (1999).
11. D. Fonseca, A. Cartaxo, and P. Monteiro, Proc. Optoelectron. **153,** 145 (2006).
12. Standard ECMA-368 "High Rate UltraWideband PHY and MAC Standard" (2007).
13. T. Alves and A. Cartaxo, Opt. Express **17,** 18714 (2009).
14. T. Alves and A. Cartaxo, J. Lightwave Technol. **30,** 1587 (2012).